Nonendpoint Majorana bound states in an extended Kitaev chain

Xuan Zhang,[1] Cheng-Ming Miao,[1] Qing-Feng Sun,[2,3,*] and Ying-Tao Zhang[1,†]
[1]*College of Physics, Hebei Normal University, Shijiazhuang 050024, China*
[2]*International Center for Quantum Materials, School of Physics, Peking University, Beijing 100871, China*
[3]*Hefei National Laboratory, Hefei 230088, China*

(Received 17 January 2024; revised 22 April 2024; accepted 26 April 2024; published 7 May 2024)

We study the energy levels and transport properties of an extended Kitaev chain with a phase gradient. It is demonstrated that the hopping phase difference can effectively induce the generation of Majorana bound states, which are located at the nonendpoint sites of the chain. The number and position of the nonendpoint Majorana bound states can be modulated by the hopping phase difference and initial hopping phase, respectively. In addition, we propose a protocol to realize topological braiding operation by exchanging the positions of two Majorana bound states in the extended Kitaev ring. Furthermore, we also implement the braiding of any two of the multiple Majorana bound states in the extended Kitaev double rings.

DOI: 10.1103/PhysRevB.109.205119

I. INTRODUCTION

Majorana bound states (MBSs) are zero-energy quasiparticles obeying non-Abelian statistics [1–6], which means that exchanging two MBSs results in a transformation depending on the order of the exchange. These properties make them ideal candidates for the realization of topological quantum computation [2,7]. There have been many theoretical proposals suggesting that MBSs exist in the vortex core of p-wave topological superconductors or at the ends of one-dimensional topological superconductors [1,4,8–12]. Although experiments show signatures expected for MBSs, the various possibilities make the interpretation challenging [13–17]. Therefore, detecting and braiding MBSs still remain an important and open challenge. In a rigorous one-dimensional system, two MBSs cannot bypass each other for braiding. Thus, some artificial two-dimensional platforms have been proposed to avoid mixing MBSs, such as T/Y junctions, quantum dots, and so on [18–22]. All these schemes inevitably require the aid of other chains or dots and are difficult to extend to braiding multiple MBSs since they are located at the endpoints of the one-dimensional chains.

In this paper, we investigate the energy levels and transport properties of an extended Kitaev chain with a phase gradient. We find that MBSs are bound at nonendpoint sites of the extended Kitaev chain in the presence of a hopping phase difference, and their number and position can be adjusted by the hopping phase difference and initial hopping phase. Furthermore, we show that the exchange of the positions of two MBSs completes the quantum braiding process in an extended Kitaev ring, which is always topologically protected by an energy gap.

II. MODEL AND HAMILTONIAN

We consider an extended Kitaev chain in which the hopping phases and p-wave superconducting phases are site dependent and linearly increasing, as shown in Fig. 1. The Hamiltonian of the extended Kitaev chain can be described as [1]

$$H_C = -\mu \sum_{n=1}^{N} c_n^\dagger c_n - t \sum_{n=1}^{N-1} e^{i\phi_n} (c_n^\dagger c_{n+1} + \text{H.c.}) + \Delta \sum_{n=1}^{N-1} e^{i\theta_n} (c_n c_{n+1} + \text{H.c.}), \quad (1)$$

where $c_n^\dagger$ (c_n) is the fermionic creation (annihilation) operator at site n and the total number of sites is chosen to be N. t is the nearest-neighbor hopping strength amplitude, which is chosen to be the unit of energy in our calculations. μ is the chemical potential, and Δ is the p-wave pairing amplitude. The phases of hopping and superconducting between site n and site $n+1$ are $\phi_n = \phi_1 + \frac{n-1}{N-1}\delta\phi$ and $\theta_n = \theta_1 + \frac{n-1}{N-1}\delta\theta$, respectively. $\delta\phi = \phi_{N-1} - \phi_1$ ($\delta\theta = \theta_{N-1} - \theta_1$) is the phase difference between the first and last hopping (superconducting) phases, and ϕ_1 (θ_1) is the initial hopping (superconducting) phase.

III. REALIZATION OF THE NONENDPOINT MAJORANA BOUND STATES

In Fig. 2(a), we calculate the energy levels of the extended Kitaev chain with open boundary conditions as a function of the hopping phase difference $\delta\phi$. The total number of sites is chosen to be $N = 200$. Considering the electron and hole degrees of freedom, the total number of states is $2N$. We show the energy structures of $E \in [-0.4t, 0.4t]$ in Fig. 2(a). We can see that the twofold-degenerate zero-energy states emerge at $\delta\phi = 0.25\pi$. The degeneracy of the zero-energy

*sunqf@pku.edu.cn
†zhangyt@mail.hebtu.edu.cn

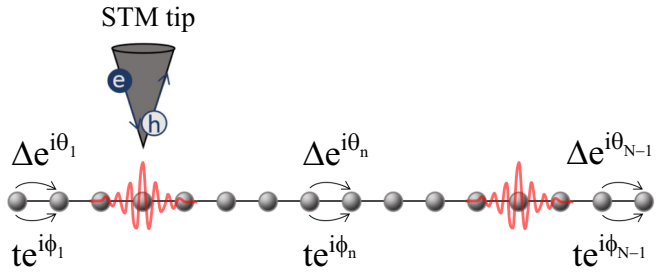

FIG. 1. Schematic of an extended Kitaev chain with site-dependent hopping and superconducting phase. $te^{i\phi_n}$ and $\Delta e^{i\theta_n}$ are hopping and superconducting terms between site n and site $n+1$, respectively. N is the total number of sites. The STM tip can scan along whole the chain. The red curves represent MBSs.

states increases in pairs with the increase of the hopping phase difference. Furthermore, we plot the energy levels with different hopping phase differences in Figs. 2(b)–2(d). It is shown that there are two zero-energy in-gap states (red dots), the probability distribution of which is highlighted in the inset of Fig. 2(b). We can see that the zero-energy in-gap states are not located at the endpoint positions of the superconducting chain. The hopping phase difference is the key factor to induce the nonendpoint MBSs protected by particle-hole symmetry, as shown in Figs. 2(a) and 2(b). It is worth noting that the zero-energy in-gap states are the MBSs because they are composed of electrons and holes each contributing half

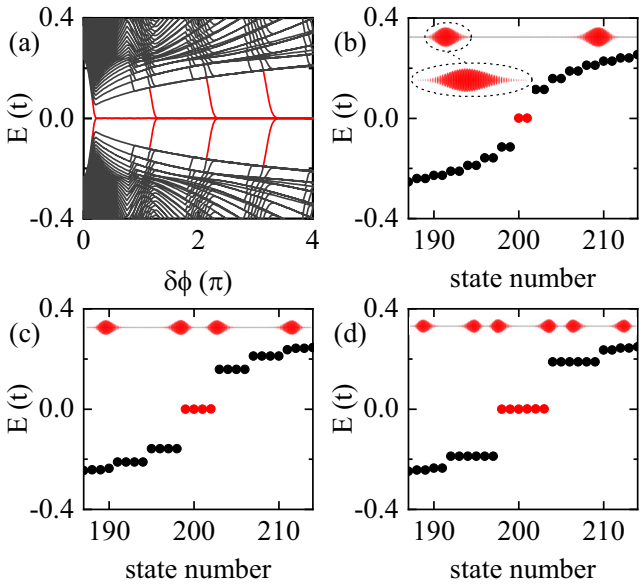

FIG. 2. (a) Band structure for the Kitaev chain as a function of hopping phase difference $\delta\phi$. The energy structures within the energy gap are highlighted in red. (b)–(d) Energy levels of the Kitaev chain with different hopping phase differences: $\delta\phi = \pi$ in (b), $\delta\phi = 2\pi$ in (c), and $\delta\phi = 3\pi$ in (d). The red dots represent the zero-energy MBSs whose probability distributions are plotted in the inset, with details enlarged in the dashed ellipse in (b). The area of the red ellipses is proportional to the modulus of the wave function. The parameters are set to be $\mu = 1$, $t = 1$, $\Delta = 1$, $\phi_1 = 0.5\pi$, $\theta_1 = 0$, $\delta\theta = 0$, and $N = 200$.

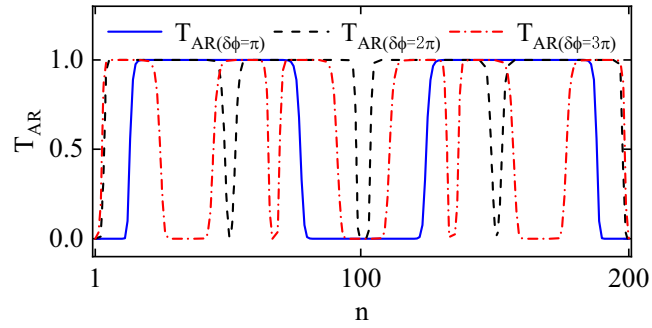

FIG. 3. Andreev reflection coefficient T_{AR} as a function of STM tip connected sites n with $\delta\phi = \pi$ (blue solid line), 2π (black dashed line), and 3π (red dot-dashed line). The energy of the incident electron is $E = 0$, and the other parameters are the same as those in Fig. 2(a).

probability. However, for the hopping phase differences $\delta\phi = 2\pi$ and $\delta\phi = 3\pi$, the four- and six-degeneracy MBSs appear, the wave function of which is distributed over nonendpoint positions of the extended Kitaev chain, as shown in Figs. 2(c) and 2(d). Our results demonstrate that nonendpoint MBSs can be induced in the extended Kitaev chain with the hopping phase difference. In addition, the number of nonendpoint MBSs can be adjusted by the magnitude of the hopping phase difference.

It is well known that a MBS can lead to a perfect Andreev reflection ($T_{AR} = 1$), a process of converting an incoming electron into an outgoing hole [23–26]. Thus, the scanning tunneling microscope (STM) spectroscopic mapping can be taken as the single Majorana detector. To detect the location of the MBSs, we imagine that an STM tip is employed to scan each lattice site n of the extended Kitaev chain (see Fig. 1). We employ the nonequilibrium Green's function method [27,28] to calculate the Andreev reflection coefficient of the extended Kitaev chain connected by the STM tip. The Andreev reflection coefficient can be described as $T_{AR}(E) = \mathrm{Tr}[\Gamma_{ee} G^r_{eh} \Gamma_{hh} G^a_{he}]$, where the linewidth function Γ and the Green's function $G^{r(a)}$ are expressed in the Nambu representation, with e and h representing the electron and hole components [27,28]. To calculate the coefficients above, we need the matrix of the surface Green's function g of the STM tip [29]. Then, by combining it with the coupling Hamiltonian between the extended Kitaev chain and the STM tip, we can calculate the retarded self-energy $\Sigma^r = t_{STM} g^r t_{STM}$, in which t_{STM} is the coupling strength between the extended Kitaev chain and the STM tip and g^r is the retarded surface Green's function of the STM tip. The linewidth function can be obtained as $\Gamma(E) = i[\Sigma^r - (\Sigma^r)^\dagger]$. Finally, with the Dyson equation, the retarded and advanced Green's functions of the extended Kitaev chain can be expressed as $G^r(E) = [G^a(E)]^\dagger = [E - H_C - \Sigma^r]^{-1}$.

In Fig. 3, we plot the Andreev reflection coefficient T_{AR} as a function of connection site n of the extended Kitaev chain with different hopping phase differences, $\delta\phi = \pi$, 2π, and 3π. Figure 3 shows that the perfect Andreev reflection coefficient $T_{AR} = 1$ occurs when the STM tip scans the nonendpoint sites of the chain, while no Andreev reflection, with $T_{AR} = 0$, occurs when scanning with the STM tip to the end sites of the

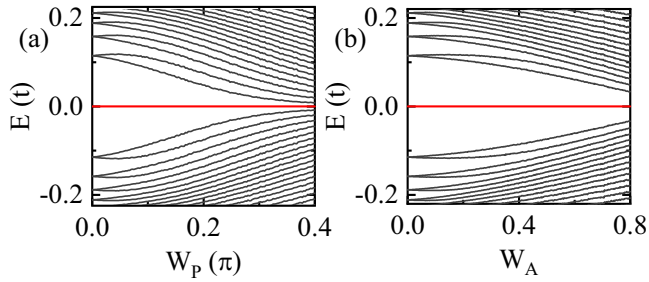

FIG. 4. The energy spectrum of the extended Kitaev chain vs (a) phase disorder strength W_P and (b) Anderson disorder strength W_A. The zero-energy states are denoted by the red lines. The parameters are the same as those in Fig. 2(b).

chain. The number and position of the perfect reflection coefficient plateau $T_{\mathrm{AR}} = 1$ are consistent with the number and distribution position of zero-energy nonendpoint bound states in the insets of Figs. 2(b)–2(d). The above results provide lateral evidence that the zero-energy nonendpoint bound states are MBSs whose numbers can be modulated by the hopping phase difference.

To verify the robustness of the in-gap MBSs, we plot the energy spectrum of the Kitaev chain versus the phase disorder strength W_P and Anderson disorder strength W_A in Figs. 4(a) and 4(b), respectively. In Fig. 4(a), the phase disorder ω_n^P is added to the hopping phase ϕ_n in Eq. (1). In Fig. 4(b), the Anderson disorder term $\sum_{n=1}^{N} \omega_n^A c_n^\dagger c_n$ is added to the Hamiltonian in Eq. (1). $\omega_n^{P(A)}$ is randomly and uniformly distributed in the interval $[-W_{P(A)}, W_{P(A)}]$. All the curves are averaged over 1000 random configurations, which is enough to obtain reasonable results. With the increasing of $W_{P(A)}$, the energy gap gradually becomes smaller, but the zero-energy states (red lines) always hold (see Fig. 4). The above results show that moderate phase disorder and Anderson disorder do not suppress the appearance of in-gap MBSs but could reduce the energy gap. It can be concluded that the MBSs are robust against the phase disorder and Anderson disorder.

IV. BRAIDING OF THE NONENDPOINT MAJORANA BOUND STATES

Naturally, we consider connecting the first and last sites of the one-dimensional chain with nonendpoint MBSs in a superconducting ring, as shown in Fig. 5(a). The Hamiltonian for the extended Kitaev ring can be written by adding two terms to Eq. (1):

$$H_R = H_C - te^{i\phi_N} c_N^\dagger c_1 + \Delta e^{i\theta_N} c_N c_1 + \mathrm{H.c.}, \qquad (2)$$

where the two added terms represent the hopping and the pairing interaction between the first and last sites of the chain. The hopping (superconducting) phase between site n and site $n+1$ is rewritten as $\phi_n = \phi_1 + \frac{n-1}{N}\delta\phi$ ($\theta_n = \theta_1 + \frac{n-1}{N}\delta\theta$), in which the phase difference between the first and last hopping (superconducting) phases is denoted by $\delta\phi = \phi_N - \phi_1$ ($\delta\theta = \theta_N - \theta_1$). The other parameters are consistent with those in Eq. (1).

In Figs. 5(b)–5(f), we calculate the energy levels of the Kitaev ring with different initial hopping phases ϕ_1. Figure 5(b)

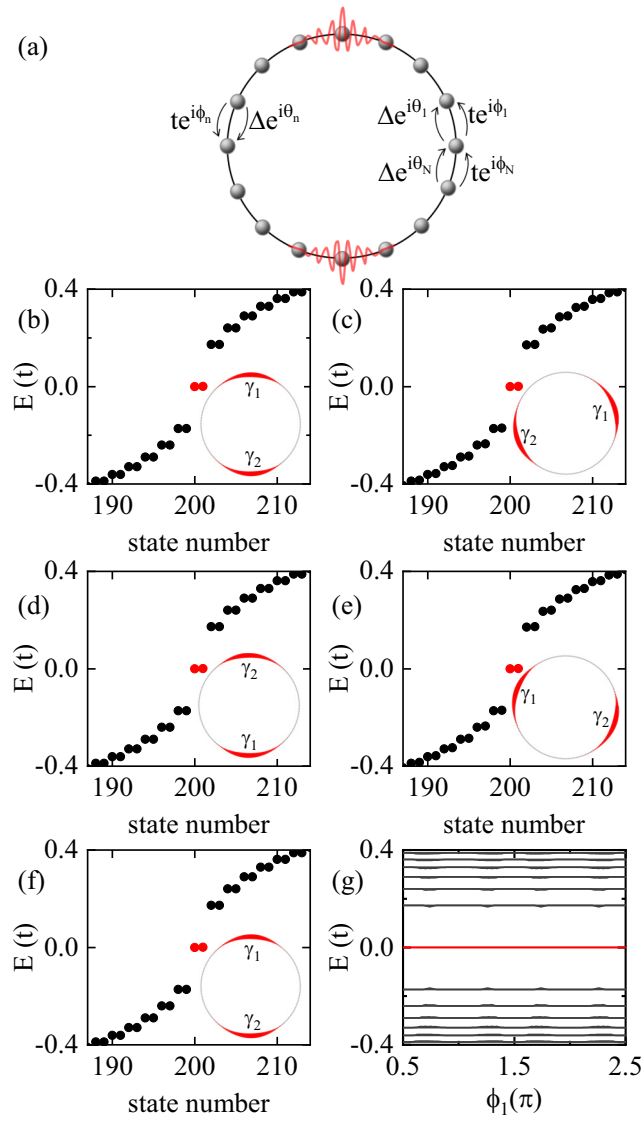

FIG. 5. (a) Schematic of the extended Kitaev ring with site-dependent hopping and superconducting phase. The red curves represent MBSs. (b)–(f) Energy levels of Kitaev ring with different initial hopping phases: $\phi_1 = 0.5\pi$ in (b), $\phi_1 = 0.7\pi$ in (c), $\phi_1 = \pi$ in (d), $\phi_1 = 1.3\pi$ in (e), and $\phi_1 = 1.5\pi$ in (f). The red dots represent the in-gap MBSs; the probability distribution of the MBSs is plotted in the inset. The area of the red ellipses is proportional to the modulus of the wave function. (g) Band structure for the Kitaev ring as a function of the initial hopping phase ϕ_1. The red line indicates the Majorana zero-energy bands, which always remain separate from the other bands (black lines). The other parameters are set to be $\mu = 1.4$, $t = 1$, $\Delta = 1$, $\delta\phi = \pi$, $\theta_1 = 0$, $\delta\theta = \pi$, and $N = 200$.

shows that two zero-energy in-gap MBSs (red dots) are still present in the extended Kitaev ring for $\phi_1 = 0.5\pi$. Since MBSs are at the nonendpoints of the extended Kitaev chain, they do not couple or disappear when the chain is linked head to tail. The two zero-energy eigenvalues of the system are denoted as $\varepsilon_{1,2}$, with the corresponding eigenstates $|\phi_{\varepsilon_{1,2}}\rangle$. Theoretically, the isolated Majorana fermions γ_1 and γ_2 can be obtained with combinations of these eigenstates, i.e., $|\phi_{\gamma_{1,2}}\rangle = (1/\sqrt{2})(|\phi_{\varepsilon_1}\rangle \pm |\phi_{\varepsilon_2}\rangle)$. At $\phi_1 = 0.5\pi$, γ_1 and γ_2 arise at the

top and bottom positions of the Kitaev ring, respectively [see the inset of Fig. 5(b)]. These two MBSs can be considered our initial state in the topological braiding process. If we increase the initial phase to $\phi_1 = 0.7\pi$, the two zero-energy in-gap MBSs remain [see Fig. 5(c)], but the positions of γ_1 (γ_2) move to the top right (bottom left) sites of the Kitaev ring, as shown in the inset of Fig. 5(c). This indicates that the positions of the MBSs can be adjusted by changing the initial hopping phase. Until $\phi_1 = \pi$, two MBSs, γ_1 and γ_2, arise at the bottom and top positions of the Kitaev ring, respectively. The spatial positions of γ_1 and γ_2 are mutually swapped, as displayed in the inset of Fig. 5(d). The braiding operation can be represented by the unitary operator $U(\gamma_1, \gamma_2) = \exp(-\frac{\pi}{4}\gamma_1\gamma_2)$. The MBSs can be transformed as $\gamma_1 \to \gamma_2$ and $\gamma_2 \to -\gamma_1$ [8]. To implement an entire topological braiding process, we continue to increase the initial hopping phase to $\phi_1 = 1.3\pi$ and $\phi_1 = 1.5\pi$. Figures 5(e) and 5(f) show that two zero-energy in-gap MBSs (red dots) always appear. As shown in the inset of Fig. 5(e), γ_1 and γ_2 are localized at the top left and bottom right positions of the Kitaev ring, respectively. Until $\phi_1 = 1.5\pi$, MBSs γ_1 and γ_2 are bounded at the top and bottom positions of the Kitaev ring, respectively [see the inset of Fig. 5(f)]. In Video 1 of the Supplemental Material [30], we show an animation of the entire braiding process with the increase of ϕ_1 from 0.5π to 1.5π. Over the entire braiding process, the spatial positions of γ_1 and γ_2 can be swapped twice, and the system returns to its initial state. After the exchange process, both MBSs γ_1 and γ_2 accumulate a π Berry phase and experience a sign flip, with $\gamma_1 \to -\gamma_1$ and $\gamma_2 \to -\gamma_2$. It is worth noting that the positions of γ_1 and γ_2 are exchanged without spatial collision. In order to observe whether the two MBSs are excited throughout the entire braiding process, we plot the energy levels of the extended Kitaev ring as a function of the initial hopping phase ϕ_1 [see Fig. 5(g)]. We can see that the zero-energy MBSs (red line) remain stable throughout the variation of ϕ_1. The isolated zero-energy MBSs can completely prevent mixing with other states (black lines) by an energy gap $(-0.17t, 0.17t)$. The braiding process can be considered to be approximately adiabatic, as long as the variation of ϕ_1 is slower than 4.1×10^{13} Hz when $t = 1$ eV. Thus, our results validate the stability of the braiding process in the extended Kitaev ring. Moreover, the two MBSs can also be exchanged counterclockwise by changing ϕ_1 from 1.5π to 0.5π.

By using the above extended Kitaev ring, we can also realize the braiding process of multiple MBSs. For example, in order to obtain an efficient braiding process of four MBSs, we set the phase differences $\delta\phi = \delta\theta = 2\pi$. By increasing the initial hopping phase ϕ_1, the four MBSs rotate in the ring. For $\phi_1 \in [0, 2\pi]$, the spatial positions of γ_1 (γ_4) and γ_3 (γ_2) are swapped twice, and the system returns to its initial state (see the Appendix). The combination of electron tunneling and rotation can identify a novel braiding operator [31]. The braiding operations can be assisted by the tunneling of electrons into or out of the MBSs [31].

To enable more elementary gate operations, we design Kitaev double rings composed of Kitaev rings R_1 and R_2. The Hamiltonian of the extended Kitaev double rings can be written as $H_D = H_{R_1} + H_{R_2} + H_t$. H_{R_1} and H_{R_2} are the Hamiltonians of Kitaev rings R_1 and R_2, which are described by

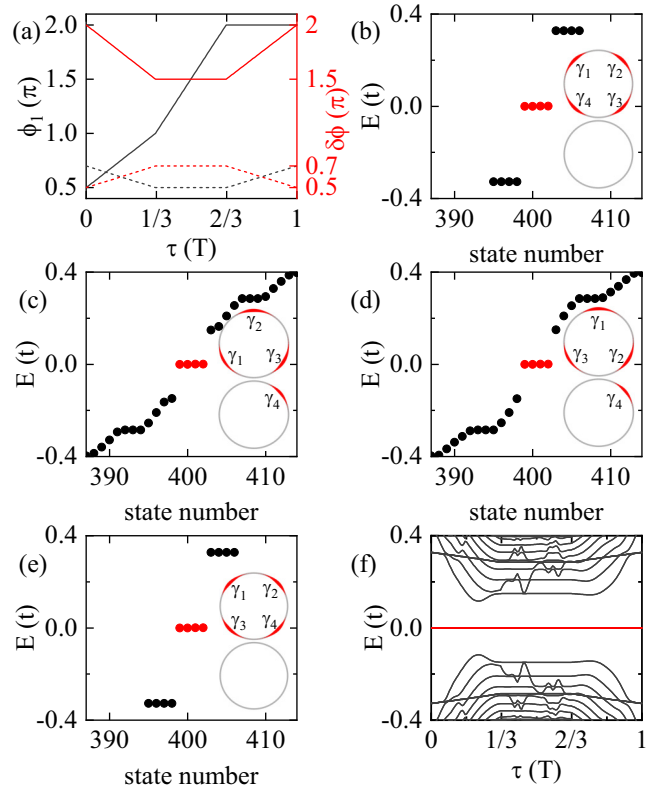

FIG. 6. (a) Initial hopping phase $\phi_1^{1,2}$ (black lines) and hopping phase difference $\delta\phi^{1,2}$ (red lines) vs time τ in the Kitaev double rings. The solid and dashed lines show the variation of the parameters in rings R_1 and R_2, respectively. (b)–(e) Energy levels of the Kitaev double rings with different times: $\tau = 0$ in (b), $\tau = T/3$ in (c), $\tau = 2T/3$ in (d), and $\tau = T$ in (e). The red dots represent the in-gap MBSs; the probability distribution of the MBSs is plotted in the inset. The area of the red ellipses is proportional to the modulus of the wave function. (f) Band structure of the Kitaev double rings as a function of time τ. The red line indicates the zero-energy MBSs, which always remain separate from the other states (black lines). The parameters of rings R_1 and R_2 are set to be $\mu_1 = 1.4$, $\theta_1^1 = 0$, $\delta\theta^1 = 1.5\pi$, and $N_1 = 200$ and $\mu_2 = 0.6$, $\theta_1^2 = 1.5\pi$, $\delta\theta^2 = 0.5\pi$, and $N_2 = 200$, respectively. The other parameters of the double rings are the same: $t = 1$, $t_1 = 1$, and $\Delta = 1$.

Eq. (2). The coupling Hamiltonian H_t between the two Kitaev rings is given by

$$H_t = -t_1 c^\dagger_{n_1} c_{n'_{N_2}} - t_1 c^\dagger_{n_{N_1}} c_{n'_1} + \text{H.c.}, \tag{3}$$

where $c^\dagger_{n_\xi}$ and $c_{n'_{\xi'}}$ are the creation operator for ring R_1 and annihilation operator for ring R_2, respectively. $\xi = 1, N_1$ ($\xi' = 1, N_2$) are the two coupling sites for Kitaev ring R_1 (R_2). t_1 is the coupling strength.

To implement topological braiding, we tune the time-dependent intensities of the initial hopping phase $\phi_1^{1,2}$ and hopping phase difference $\delta\phi^{1,2}$, as displayed in Fig. 6(a). In Figs. 6(b)–6(f), we calculate the energy levels of the Kitaev double rings with different times τ. The braiding protocol takes four steps in T time to spatially swap two neighboring MBSs γ_3 and γ_4: (1) At $\tau = 0$, we set $\phi_1^1 = 0.5\pi$, $\phi_1^2 = 0.7\pi$, $\delta\phi^1 = 2\pi$, and $\delta\phi^2 = 0.5\pi$. Figure 6(b) shows that four

zero-energy in-gap MBSs (red dots) are present in the extended Kitaev double rings. γ_1, γ_2, γ_3, and γ_4 arise at four positions of the upper ring, R_1 [see the inset of Fig. 6(b)]. These four MBSs can be considered our initial state in the topological braiding process. (2) At $\tau = T/3$, the initial hopping phase and hopping phase difference change to $\phi_1^1 = \pi$, $\phi_1^2 = 0.5\pi$, $\delta\phi^1 = 1.5\pi$, and $\delta\phi^2 = 0.7\pi$. The four zero-energy MBSs remain [see Fig. 6(c)], but the position of γ_4 moves to ring R_2. The remaining three MBSs, γ_1, γ_2, and γ_3, are located in the bottom left, top, and bottom right sites of ring R_1, respectively [see the inset of Fig. 6(c)]. (3) For $\tau \in [T/3, 2T/3]$, we increase only ϕ_1^1 of ring R_1 from π to 2π and keep the rest of the parameters unchanged. It can be seen that four MBSs remain at $\tau = 2T/3$, as shown in Fig. 6(d). The inset of Fig. 6(d) shows that the position of γ_4 remains unchanged in ring R_2, while the positions of γ_1, γ_2, and γ_3 are turned counterclockwise in ring R_1 to the top, bottom right, and bottom left sites, respectively. (4) For $\tau \in [2T/3, T]$, we leave the initial hopping phase of ring R_1 unchanged at $\phi_1^1 = 2\pi$ and change the remaining three parameters to $\phi_1^2 = 0.7\pi$, $\delta\phi^1 = 2\pi$, and $\delta\phi^2 = 0.5\pi$. We can see from Fig. 6(e) that the four MBSs still emerge, as shown by red dots. The inset of Fig. 6(e) shows that MBSs γ_1, γ_2, γ_3, and γ_4 are bounded at the top left, top right, bottom left, and bottom right sites of ring R_1, respectively. The spatial positions of γ_3 and γ_4 are mutually swapped, and the spatial positions of γ_1 and γ_2 remain unchanged [see the insets of Figs. 6(b) and 6(e)]. In Video 2 of the Supplemental Material [30], we show an animation of the braiding process when the time τ increases from 0 to T, as shown in Fig. 6(a).

In order to observe whether the four MBSs are excited throughout the entire braiding process, we plot the energy levels of the extended Kitaev double rings as a function of the time τ [see Fig. 6(f)]. We can see that the zero-energy MBSs (red line) remain stable throughout the variation of τ. The isolated zero-energy MBSs can completely prevent mixing with other states (black lines) by an energy gap. Thus, our results validate the stability of the braiding process in the extended Kitaev double rings. Furthermore, any two adjacent MBSs of the four MBSs can be swapped in the extended Kitaev double rings, so we can construct a braiding operation for unary gates such as Pauli gates, S gates, and Hadamard gates. To detect the MBSs in double rings, the differential conductance at each site can be measured by a STM. In addition, two of the six MBSs can be swapped pairwise to obtain the braiding operations of binary gates such as controlled-NOT gates. Thus, a variety of braiding schemes can be designed in a multiple-ring system.

Finally, we present the possibility of an experimental realization of the proposed setup. The phases in Eq. (1) are determined by two initial phases, ϕ_1 and θ_1, and two phase differences, $\delta\phi$ and $\delta\theta$. The value of the initial superconducting phase θ_1 does not affect the appearance and positions of nonendpoint MBSs. The gauge transformation $c_n \to c_n e^{i\theta_n/2}$ eliminates the phase from the superconducting terms, in exchange for adding the complex amplitude $e^{i(\theta_n-\theta_{n+1})/2}$ to the hopping term from site n to site $n+1$ [32]. The superconducting phase gradient and the initial hopping phase can be converted into each other. The superconducting phase difference $\delta\theta$ and initial hopping phase ϕ_1 can be tuned by persistent spin current and magnetic flux [26,33–35]. Experimentally, a constant force can be introduced around the smaller perimeter of the hopping torus to adiabatically realize the gradient of ϕ_n, $F \propto \partial_t \phi_n$ [36,37]. It gives rise to a quantized Hall current perpendicular to the introduced force. Alternatively, superconducting charge qubits consisting of a dc superconducting quantum interference device with two identical Josephson junctions can be placed at each site. Hence, a phase gradient can be introduced experimentally to realize phase settings. A lattice-dependent gradient current induces the emergence and movement of nonendpoint MBSs.

V. CONCLUSIONS

In this work, we investigated the energy levels and transport properties of an extended Kitaev chain with a site-dependent linearly increasing hopping phase and p-wave superconducting phase. We demonstrated that the controlled number of nonendpoint MBSs can be induced in the chain with the hopping phase difference. Furthermore, we proposed a protocol to implement the pairwise exchange of MBSs in an extended Kitaev ring and the swap of any two MBSs of the multiple MBSs in the extended Kitaev double rings. Importantly, MBSs remain stable throughout the braiding process, as evidenced by the fact that the MBSs can be completely protected from mixing with other states by an energy gap.

ACKNOWLEDGMENTS

This work was financially supported by the National Natural Science Foundation of China (Grants No. 12074097, No. 11921005, and No. 12374034), the Innovation Program for Quantum Science and Technology (Grant No. 2021ZD0302403), and the Strategic Priority Research Program of Chinese Academy of Sciences (Grant No. XDB28000000) .

X.Z. and C.-M.M. contributed equally to this work.

APPENDIX: BRAIDING OF MULTIPLE MAJORANA BOUND STATES

In order to obtain an efficient braiding process of four MBSs in one extended Kitaev ring, we plot the energy levels and wave function distribution with phase differences $\delta\phi = \delta\theta = 2\pi$ in Fig. 7. Figures 7(a)–7(e) show that there are always four zero-energy in-gap MBSs (red and blue dots) that appear with different initial hopping phases. For every MBS, the probability of the wave functions is highlighted in the insets of Figs. 7(a)–7(e) by the corresponding color. Here, the four zero-energy eigenvalues of the system are denoted as $\varepsilon_{1,2,3,4}$, and the corresponding eigenstates are $|\phi_{\varepsilon_{1,2,3,4}}\rangle$. As shown in Fig. 7(a), the zero-energy eigenstates $|\phi_{\varepsilon_2}\rangle$ and $|\phi_{\varepsilon_3}\rangle$ (in blue) correspond to the excitations of γ_1 and γ_4, while the zero-energy eigenstates $|\phi_{\varepsilon_1}\rangle$ and $|\phi_{\varepsilon_4}\rangle$ (in red) correspond to the excitations of γ_2 and γ_3. Theoretically, the isolated Majorana fermions can be obtained by combinations of these zero-energy eigenstates, i.e., $|\phi_{\gamma_{1,4}}\rangle = (1/\sqrt{2})(|\phi_{\varepsilon_2}\rangle \pm |\phi_{\varepsilon_3}\rangle)$ and $|\phi_{\gamma_{2,3}}\rangle = (1/\sqrt{2})(|\phi_{\varepsilon_1}\rangle \pm |\phi_{\varepsilon_4}\rangle)$. At $\phi_1 = 0$, γ_1 and γ_4 arise in the top right and bottom right positions of the Kitaev ring, while γ_2 and γ_3 arise in the top left and bottom left

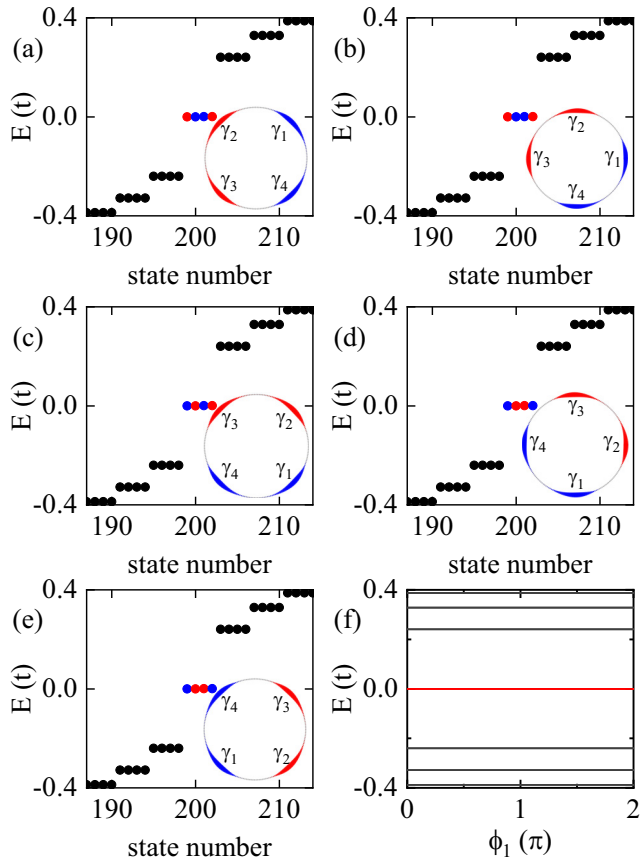

FIG. 7. (a)–(e) Energy levels of a Kitaev ring with different initial hopping phases: $\phi_1 = 0$ in (a), $\phi_1 = 0.25\pi$ in (b), $\phi_1 = 0.5\pi$ in (c), $\phi_1 = 0.75\pi$ in (d), and $\phi_1 = \pi$ in (e). The red and blue dots represent the in-gap MBSs; the probability distribution of the MBSs is plotted in the inset. (f) Band structure of the Kitaev ring as a function of the initial hopping phase ϕ_1 with phase differences $\delta\phi = \delta\theta = 2\pi$. The other parameters are the same as those in Fig. 5(b).

positions of the Kitaev ring, respectively [see the inset of Fig. 7(a)]. These four MBSs can be considered our initial state in the topological braiding process. The positions of γ_1, γ_4, γ_2, and γ_3 are moved to be the right, bottom, left, and top sites of the extended Kitaev ring for $\phi_1 = 0.25\pi$, as shown in the inset of Fig. 7(b). By increasing the initial hopping phase to $\phi_1 = 0.5\pi$, γ_1 and γ_4 arise in the bottom right and bottom left positions, and γ_2 and γ_3 arise in the top right and top left positions of the Kitaev ring, as displayed in the inset of Fig. 7(c). As shown in the inset of Fig. 7(d), γ_1, γ_4, γ_2, and γ_3 are localized in the bottom, left, top, and right positions of the Kitaev ring, respectively. Until $\phi_1 = \pi$, γ_1, γ_4, γ_2, and γ_3 are bounded at the bottom left, top left, bottom right, and top right positions of the Kitaev ring, respectively [see the inset of Fig. 7(e)]. The spatial positions of γ_1 (γ_4) and γ_3 (γ_2) are mutually swapped. The braiding operation can be represented by the unitary operators $U(\gamma_1, \gamma_3) = \exp(-\frac{\pi}{4}\gamma_1\gamma_3)$ and $U(\gamma_4, \gamma_2) = \exp(-\frac{\pi}{4}\gamma_4\gamma_2)$. The MBSs can be transformed as $\gamma_1 \to \gamma_3$, $\gamma_3 \to -\gamma_1$ and $\gamma_4 \to \gamma_2$, $\gamma_2 \to -\gamma_4$ [8]. For $\phi_1 \in [0, 2\pi]$, the spatial positions of γ_1 (γ_4) and γ_3 (γ_2) are swapped twice, and the system returns to its initial state. The combination of the electron tunneling and rotation can reveal a novel braiding operator [31]. The braiding operations can be assisted by tunneling of electrons into or out of the MBSs [31].

In order to observe whether the four MBSs are excited throughout the entire braiding process, we plot the energy levels as a function of the initial hopping phase ϕ_1 in Fig. 7(f). We can see that the fourfold-degenerate zero-energy states (red line) remain stable throughout the variation of ϕ_1. The four isolated MBSs can completely prevent mixing with other states (black lines) by an energy gap, which demonstrates that the braiding process is adiabatically changing. Our results validate that the stabilized braiding process of four MBSs was obtained by fixing the phase difference to be $\delta\phi = \delta\theta = 2\pi$ and tuning the initial hopping phase. Furthermore, MBSs can also be exchanged counterclockwise by setting $\phi_1 \in [2\pi, 0]$.

[1] A. Y. Kitaev, Phys. Usp. **44**, 131 (2001).
[2] C. Nayak, S. H. Simon, A. Stern, M. Freedman, and S. Das Sarma, Rev. Mod. Phys. **80**, 1083 (2008).
[3] F. Wilczek, Nat. Phys. **5**, 614 (2009).
[4] J. Alicea, Rep. Prog. Phys. **75**, 076501 (2012).
[5] M. Leijnse and K. Flensberg, Semicond. Sci. Technol. **27**, 124003 (2012).
[6] C. Beenakker, Annu. Rev. Condens. Matter Phys. **4**, 113 (2013).
[7] J. Alicea, Y. Oreg, G. Refael, F. von Oppen, and M. P. A. Fisher, Nat. Phys. **7**, 412 (2011).
[8] D. A. Ivanov, Phys. Rev. Lett. **86**, 268 (2001).
[9] R. M. Lutchyn, J. D. Sau, and S. Das Sarma, Phys. Rev. Lett. **105**, 077001 (2010).
[10] Y. Oreg, G. Refael, and F. von Oppen, Phys. Rev. Lett. **105**, 177002 (2010).
[11] S. Nadj-Perge, I. K. Drozdov, B. A. Bernevig, and A. Yazdani, Phys. Rev. B **88**, 020407(R) (2013).
[12] M. Hell, M. Leijnse, and K. Flensberg, Phys. Rev. Lett. **118**, 107701 (2017).
[13] D. Bagrets and A. Altland, Phys. Rev. Lett. **109**, 227005 (2012).
[14] D. Rainis, L. Trifunovic, J. Klinovaja, and D. Loss, Phys. Rev. B **87**, 024515 (2013).
[15] J. Liu, A. C. Potter, K. T. Law, and P. A. Lee, Phys. Rev. Lett. **109**, 267002 (2012).
[16] C.-X. Liu, J. D. Sau, T. D. Stanescu, and S. Das Sarma, Phys. Rev. B **96**, 075161 (2017).
[17] C. Moore, T. D. Stanescu, and S. Tewari, Phys. Rev. B **97**, 165302 (2018).
[18] T. Karzig, Y. Oreg, G. Refael, and M. H. Freedman, Phys. Rev. X **6**, 031019 (2016).
[19] Q. Yan, Y.-F. Zhou, and Q.-F. Sun, Phys. Rev. B **100**, 235407 (2019).
[20] Y.-F. Zhou, Z. Hou, and Q.-F. Sun, Phys. Rev. B **99**, 195137 (2019).
[21] R. V. Mishmash, B. Bauer, F. von Oppen, and J. Alicea, Phys. Rev. B **101**, 075404 (2020).
[22] J. Manousakis, C. Wille, A. Altland, R. Egger, K. Flensberg, and F. Hassler, Phys. Rev. Lett. **124**, 096801 (2020).
[23] Y.-T. Zhang, Z. Hou, X. C. Xie, and Q.-F. Sun, Phys. Rev. B **95**, 245433 (2017).

[24] Q. Li, Y. Han, K. Zhang, Y.-T. Zhang, J.-J. Liu, and Z. Qiao, Phys. Rev. B **102**, 205402 (2020).
[25] Y. Zhuang and Q.-F. Sun, Phys. Rev. B **105**, 165148 (2022).
[26] C.-M. Miao, Q.-F. Sun, and Y.-T. Zhang, Phys. Rev. B **105**, 085401 (2022).
[27] S.-G. Cheng, Y. Xing, J. Wang, and Q.-F. Sun, Phys. Rev. Lett. **103**, 167003 (2009).
[28] Q.-F. Sun and X. C. Xie, J. Phys.: Condens. Matter **21**, 344204 (2009).
[29] D. H. Lee and J. D. Joannopoulos, Phys. Rev. B **23**, 4997 (1981).
[30] See Supplemental Material at http://link.aps.org/supplemental/10.1103/PhysRevB.109.205119 for animations of braiding Majorana bound states.
[31] S. Park, H.-S. Sim, and P. Recher, Phys. Rev. Lett. **125**, 187702 (2020).
[32] O. Lesser, A. Saydjari, M. Wesson, A. Yacoby, and Y. Oreg, Proc. Natl. Acad. Sci. USA **118**, e2107377118 (2021).
[33] F. Pientka, A. Romito, M. Duckheim, Y. Oreg, and F. von Oppen, New J. Phys. **15**, 025001 (2013).
[34] G.-Q. Zha, L. Covaci, F. M. Peeters, and S.-P. Zhou, Phys. Rev. B **92**, 094516 (2015).
[35] A. Nava, R. Giuliano, and G. Campagnano, and D. Giuliano, Phys. Rev. B **95**, 155449 (2017).
[36] F. Grusdt and M. Höning, Phys. Rev. A **90**, 053623 (2014).
[37] F. Yang, V. Perrin, A. Petrescu, I. Garate, and K. Le Hur, Phys. Rev. B **101**, 085116 (2020).